Journal of Molecular Structure 1294 (2023) 136508

Contents lists available at ScienceDirect

Journal of Molecular Structure

journal homepage: www.elsevier.com/locate/molstr

Structure-based virtual screening of new antitumor natural berberines: Bioactivity against pancreas cancer by HIF1 inhibition effect

Matheus Nunes da Rocha [a], Márcia Machado Marinho [b], Hélcio Silva dos Santos [c], Emmanuel Silva Marinho [a,d,*], Jonas Ildefonso Junior [e], Janini Filgueira Rosas [e], Henrique Douglas Melo Coutinho [f,*]

[a] Graduate Program in Natural Sciences, Center for Science and Technology, State University of Ceará, Fortaleza, CE, Brazil
[b] Faculty of Education, Science and Letters of Iguatu, State University of Ceará, Iguatu, CE, Brazil
[c] Chemistry Department, Regional University of Cariri, Crato, CE, Brazil
[d] Group of Theoretical Chemistry and Electrochemistry, State University of Ceará, Limoeiro Do Norte, CE, Brazil
[e] CECAPE College. Av. Padre Cícero, 3917 - São José, Juazeiro do Norte - CE, 63024-015, Brazil
[f] Biological Chemistry Department, Regional University of Cariri, Crato, CE, Brazil

ARTICLE INFO

Keywords:
HIF-1 inhibition
ADME study
Pancreatic cancer
Berberine
Molecular docking

ABSTRACT

Despite medical and technological advances to contain the proliferation of pancreatic cancer, many diagnoses are late due to the high specificity of this type of cancer. Because it is asymptomatic cancer until the most advanced or terminal state, the efficiency of therapeutic actions can be reduced. HIF-1α is the factor that regulates crucial genes involved in tumor proliferation and metastasis. In this study, a virtual structure-based screening was carried out to evaluate the alignment between pharmacokinetics and pharmacodynamics against the anti-cancer mechanism of the pancreas via HIF-1α of new derivatives of the natural product berberine, a natural alkaloid based on protic isoquinoline whose antitumor effect is reported in the literature. Here, a multiparametric optimization system is used to estimate, quantitatively and topologically, the alignment between the pharmacokinetic attributes of these analogs, where it was possible to observe that the less lipophilic analogs, that is, the **1a-b** derivatives, showed better ADME viability. Furthermore, the substitution of alkyl bromide promotes an inductive electron-withdrawing effect that increases the probability of demethylation in analog **1b** and reduces the number of O-dealkylation sites, increasing the metabolic stability of the compound. The results of molecular docking suggest that the ligands with better viability of ADME also present a great affinity and specificity for the HIF-1α receptor, mainly in interactions in common with the residue of Thr 196, present in the binding site of the OGA inhibitor, constituting promising ligands in the treatment of pancreatic cancer.

1. Introduction

Despite technological and medical advances in the diagnosis and treatment of various cancers worldwide, pancreatic cancer, in particular, remains the most aggressive and lethal. In the year 2020, the mortality from pancreatic cancer reached a staggering range of 90% among affected people [1], although chemotherapy causes significant progress in treatment [2]. However, in many cases, patients present asymptomatic situations of the disease, which reduces the accuracy of diagnoses, only being identified in more advanced stages of the disease and, consequently, reducing the degree of reversibility from therapeutic actions [3].

Pancreatic neoplasms can be divided into two groups: endocrine tumors, which affect the secretion of hormones such as insulin, glucagon and somatostatin, and non-endocrine or exocrine tumors, associated with the secretion of digestive enzymes, such as trypsinogen, chymotrypsinogen, lipase and amylase [4,5]. Exocrine cancer is the most common and most aggressive. In this group, pancreatic ductal adenocarcinoma (PDAC) stands out, often diagnosed in an advanced state and metastasizes mainly to the liver and lymph nodes. In this case, anti-cancer therapies are not very effective, as the tumor acquires advanced cytoprotective mechanisms that promote drug resistance [5].

Hypoxia is a condition of a deficiency of oxygen in body tissues triggered by a malfunction or response to some abnormal function. This

* Corresponding authors.
E-mail addresses: emmanuel.marinho@uece.br (E. Silva Marinho), hdmcoutinho@gmail.com (H.D.M. Coutinho).

https://doi.org/10.1016/j.molstruc.2023.136508
Received 19 May 2023; Received in revised form 12 July 2023; Accepted 27 August 2023
Available online 28 August 2023

is a very common condition in the microenvironment of solid tumors. The Hypoxia-Inducible Factor 1α (HIF-1α) is the main regulator of cellular response to these abnormal functions. In regions of intratumoral hypoxia, HIF-1α regulates crucial genes to mediate proliferation, stem cell maintenance and the process of metastasis itself [6–8]. In this way, organic compounds that selectively modulate HIF-1α can effectively reduce the proliferation of pancreatic cancer cells.

Alkaloids, for example, are a class of organic compounds that are present as secondary metabolites in natural products and responsible for various pharmacological activities, including their anticancer therapeutic potential [9]. Alkaloids have reinvigorated the development of drugs from quinolines and isoquinolines of fundamental importance for pharmaceutical chemistry, such as morphine, codeine and berberines [10].

Berberine, also known as *Coptis rhizome*, is a natural alkaloid whose chemical structure is formed by a protic isoquinoline, called protoberberine, linked to an oxygenated substructure of benzodioxole [11] (Fig. 1). It is widely used in Chinese folk medicine and can be extracted from plant species such as Berberis, whose rich therapeutic activities include anti-Alzheimer's [12], anti-diabetic [13], anti-inflammatory [14], anti-viral [15], anti-bacterial [16] and, the one addressed in the problematic of this study, anti-cancer [9].

For this structure-based virtual screening study, a series of compounds derived from the natural product berberine were selected, whose main pharmacophore is based on the substitution of alkyl chains in the methoxylated isoquinoline substructure of the bibliographic review study by Gaba et al. [17]. These substances were evaluated in an *in vitro* cytotoxic study published by Wang et al. [18], where the addition of alkyl chains was induced by 9-O-demethylation (**1**) in high vacuum at 190 °C, where aromatic hydroxylation favored alkylation in dimethylformamide (DMF) (Fig. 2). The second group of substituted radicals (**2**) constitute more lipophilic derivatives with the addition of alkyl and O-alkyl radicals on carbon 13 of the isoquinoline substructure, under ethanol (EtOH) at 85–95 °C [19]. So far, the first group (**1**) has induced apoptosis in HeLa cell lines with a low concentration (5 μM), while the second group (**2**) has shown promise in inhibiting the proliferation of HepG2, HT-29 and BFTC905 cell lines [17].

Based on this premise, this work consists of a structure-based virtual screening study of a series of substituted alkyl berberine derivatives that raise approaches for predicting the pharmacokinetics and pharmacodynamics of new HIF-1α modulators in the treatment of pancreatic cancer based on multiparameter optimization (MPO) and molecular docking techniques.

2. Material and method

2.1. Molecular lipophilicity potential and topological analysis

Initially, the two-dimensional representation of the chemical structures of the natural product berberine and its analogs **1a-c** and **2a-b** were plotted by the long-term support version of the academic license

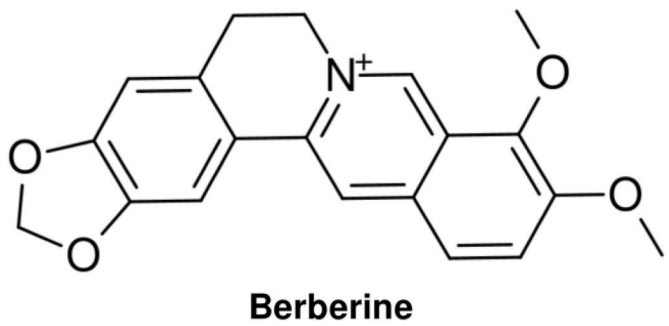

Fig. 1. Two-dimensional representation of the chemical structure of berberine.

software MarvinSketch®, version Iodine 7, Chemaxon© (https://chemaxon.com/marvin), for the calculation of the Molecular Lipophilicity Potential (MLP), as shown in Eq. (1):

$$MLP_k = \sum_{i=1}^{N} F_i \cdot f(d_{ik}) \quad (1)$$

Where N is the number of molecular fragments, F is the lipophilicity index of each fragment i, negative for hydrophilic fragments and positive for hydrophobic fragments, and $f(d_{ik})$ is a function of the spatial distance (k) between fragments i [20].

The plotted ligands were optimized using the Merck Molecular Force Field 94 (MMFF94) [21], configured for a very strict optimization limit, which returns the conformation with the lowest potential energy in kcal/mol in its prehydrogenized structure and considering bonds of intramolecular hydrogen. Then, the structures were uploaded in the Jmol Java Script program, version 10.0 (https://jmol.sourceforge.net/), for visualization of the MLP surface based on the Molecular Electrostatic Potential (MEP) plot, as shown in Eq. (2):

$$\Pi = \frac{1}{m}\sum_{i=1}^{m} |V(r_i) - \tilde{V}| \quad (2)$$

Where $V(r_i)$ is the MEP calculated at a point r_i, $\tilde{V}$ is the MEP of the complete molecular surface, including anionic and cationic substructures. The Π parameter can identify polar surface areas (PSA) and the quantitative neighborhoods of atoms [22], resulting in a surface map where the points vary from blue (hydrophilic) to red (lipophilic).

2.2. MPO desirability functions to ADME estimative

The ligands, in simplified molecular-input line-entry system (SMILES) notation, were uploaded to Java Script Marvin software for quantitative estimation of drug-likeness based on the desirability function (D) from Pfizer's Multiparameter Optimization (MPO) algorithm, expressed by the Eq. (3) [23] and analyzed by chemical intelligence in the opensource software OSIRIS DataWarrior version 5.5.0, openmolecules (https://openmolecules.org/datawarrior/):

$$D = \sum_{k=1}^{M} w_k T_k\left(x_k^0\right) \quad (3)$$

Where $T(x)$ is the order of satisfaction for a calculated physicochemical attribute k, which is inside ($x_k < x_a$) or outside ($x_b < x_k$), which includes the limits: lipophilicity by partition coefficient (logP $\leq$ 3) and distribution coefficient in physiological pH (logDpH 7.4 $\leq$ 2), Molecular Weight (MW $\leq$ 360 g/mol), Topological Polar Surface Area (40 $<$ TPSA $\leq$ 90 Å^2), H-bond donor count (HBD $\leq$ 1) and pKa from the most basic center (pKa $\leq$ 8); and w is the weighting factor of each attribute k in the final MPO score, which ranges from 0 (poor drug-likeness) to 6 (optimal drug-likeness), with favorable MPO values $>$ 5 that indicate an alignment between fundamental attributes of absorption, distribution, metabolism and excretion (ADME), which include: passive permeability (P_{app}) in Madin-Darby Canine Kidney (MDCK) cell line, passive efflux by intestinal P-glycoprotein (P-gp), metabolic stability in the Human Liver Microsome (HLM) and intrinsic clearance of the unbound systemic fraction ($CL_{int,u}$). ADME descriptors were estimated using structure-based virtual screening services on ADMETlab 2.0 (https://admetmesh.scbdd.com/) and ADMETboost – AI Drug Lab (https://ai-druglab.smu.edu/) to validate the alignment between the pharmacokinetic attributes of the ligands [24].

2.3. Site of metabolism and toxicity prediction

The ligands, converted into SMILES notation, were reported to the SMARTCyp online server (https://smartcyp.sund.ku.dk/mol_to_som) for site metabolism prediction. The test is based on a similarity test using activation energies determined by density functional theory (DFT) for more than 250 known molecules to estimate the most likely site of

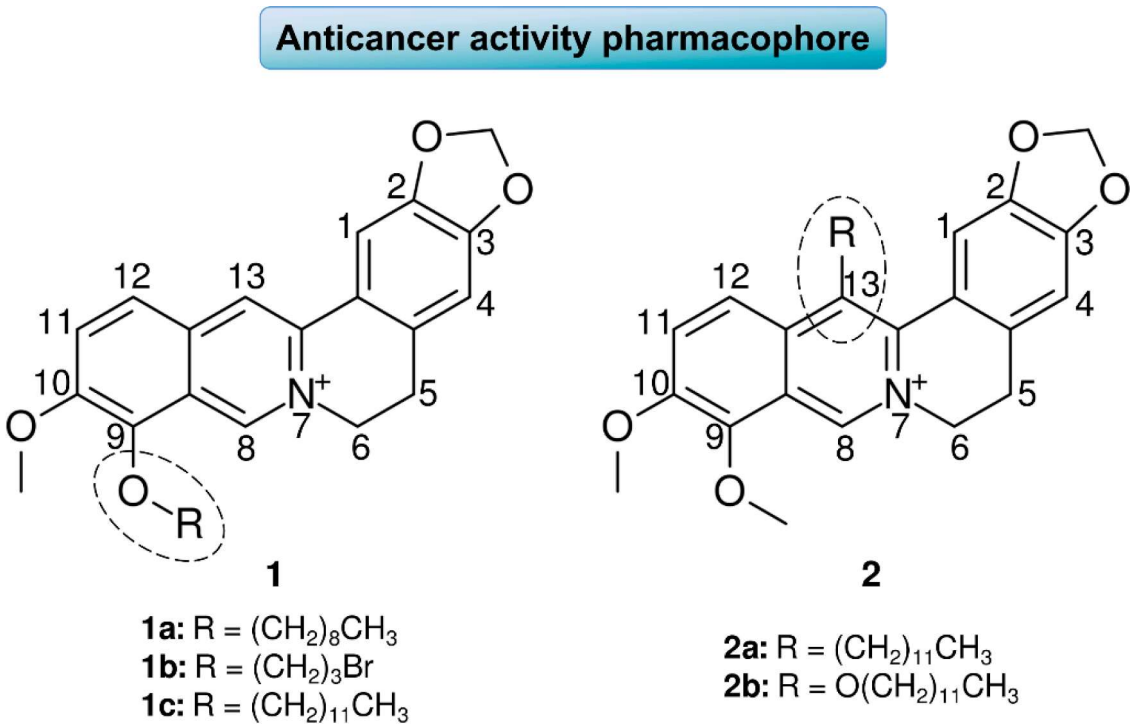

Fig. 2. Sites of alkylation as a key point for increasing the anticancer activity of berberines.

metabolism, generating a 2D probability map that was associated with the probability of the compounds are substrates of cytochrome P450 (CYP450) isoforms of types 2C9, 2D6 and 3A4 [25], and that they result in hepatotoxic damage (H—HT descriptor) of the ADME predictive test.

2.4. Molecular docking against HIF-1α receptor

With molecular docking methodology adapted from the study by Frota et al., (2022) [26], the RCSB Protein Data Bank (PDB) repository (https://www.rcsb.org/) was consulted to obtain the target called "Factor Inhibiting HIF-1α alpha in complex with HIF-1α alpha fragment peptide" (PDB ID: 1H2M) determined by X-ray diffraction (R-Value Free: 0.225, R-Value Work: 0.192 e R-Value Observed: 0.194), deposited at repository under a resolution of 2.50 Å, and classified as Transcription Activator/Inhibitor in *Homo sapiens* organism. The target preparation included the removal of N—OXALYLGLYCINE (OGA), residual water (H_2O) and sulfate and zinc ions, followed by the addition of polar hydrogens and Gasteiger charges via AutoDockTools® software [27]. The grid box had its center set at $x = 21.473$, $y = 28.353$ and $z = 28.124$, with dimensions $x = 58$, $y = 66$ and $z = 56$ using the Exhaustiveness criterion equal to 64. Finally, the AutoDockVina® [28] software performed molecular docking simulations with 20 independent simulations with 10 poses each for each molecule. The grid box parameters were adjusted for the OGA inhibitor binding site.

The "best-pose" selection criteria include : (i) Root Mean Square Deviation (RMSD) < 2.0 Å [29], as a statistical validation model; (ii) affinity energy, given by the Gibbs free energy descriptor (ΔG), within the ideality standard ≤ -6.0 kcal/mol [30]; and (iii) classification of the strengths of H-bond and hydrophobic interactions, by distances (d) Ligand-Receptor (L–R), into strong ($d < 2.5$ Å), moderate (2.5 Å $< d <$ 3.1 Å) and weak (3.1 Å $< d$) [31].

3. Results

3.1. MPO desirability and topological analysis

Pfizer's MPO system was applied to quantitatively estimate the drug-likeness of alkylated berberine derivatives, considering the maximum and minimum limits that resulted in the transformed values. In the radar graph of Fig. 3, it is possible to observe that the lipophilicity of these derivatives, either by logP or by logD at physiological pH, varies with the increase in molecular weight. Here, it is worth mentioning that the compounds with longer alkyl side chains (12 C atoms), that is, the derivatives **1c** ($(CH_2)_{11}CH_3$), **2a** ($(CH_2)_{11}CH_3$) and **2b** ($O(CH_2)_{11}CH_3$), shift outside the ideal buffered lipophilicity spectrum ($logD_{pH\ 7.4}$) estimated by the algorithm, which considers a physicochemical space for drugs, drug candidates and active substances in the CNS database of Pfizer, Inc. [23].

In Fig. 4, it is possible to note that these side chains contribute in an atomistic increment of around 0.44, with a higher lipophilicity index for the terminal carbons (0.68), within the MLP scale estimated by the atomistic logP prediction method of Chemaxon©, resulting in essentially hydrophobic molecular surface regions, where the spectrum varies from yellow to red (Fig. 5). However, they present a positively charged center as a hydrophilic region (green to blue spectra), with an atomistic

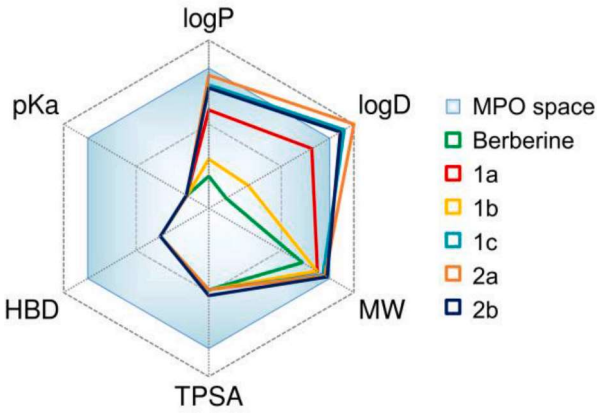

Fig. 3. Physicochemical space radar generated by Pfizer's MPO algorithm to estimate the drug-likeness of berberine and its analogs **1a-c** and **2a-b**.

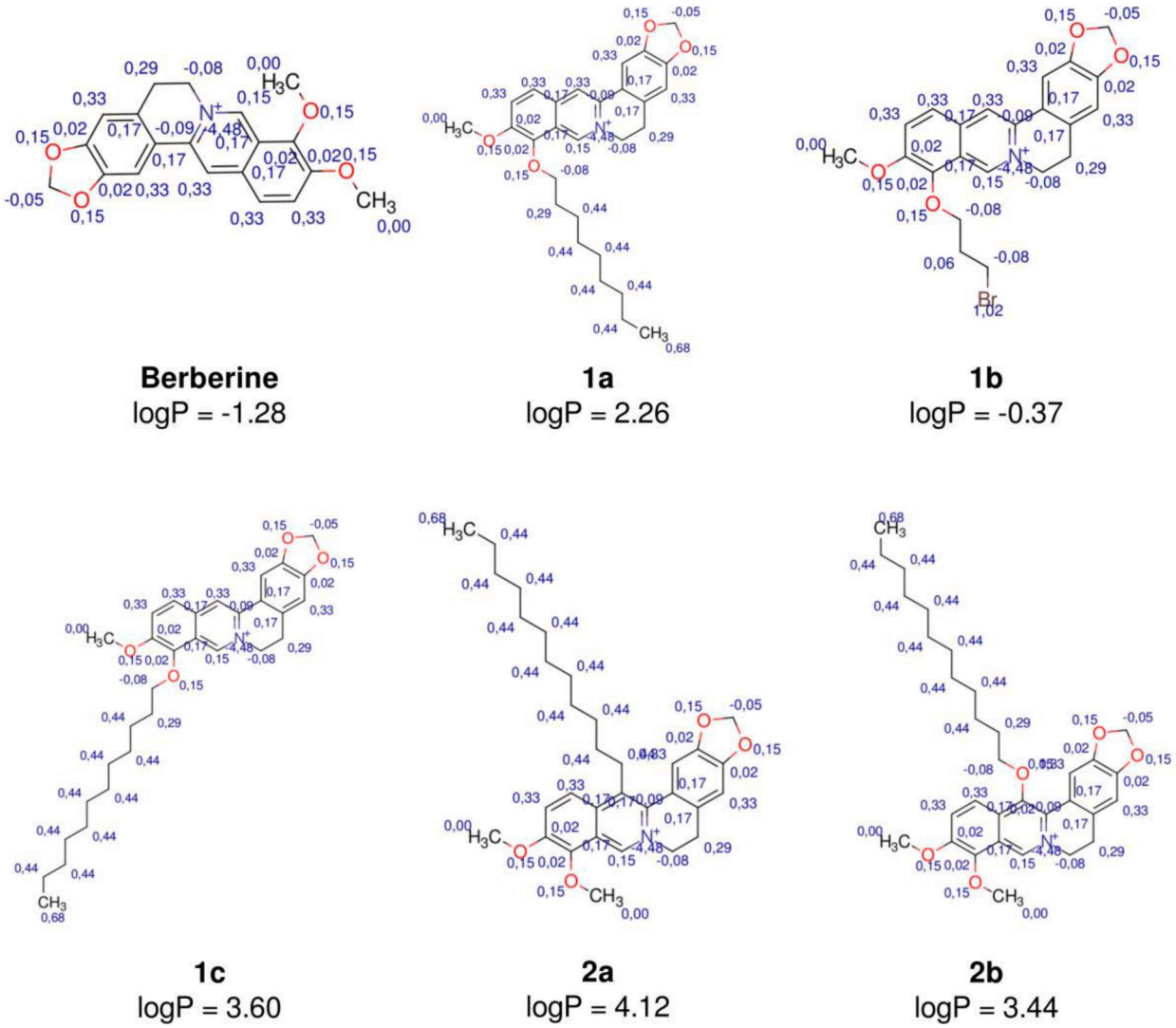

Fig. 4. Structural increments of molecular fragments in molecular lipophilicity potential (MLP) of berberine derivatives.

contribution of the order of −4.48.

The synthetic derivatives, as well as the natural product berberine, are within a calculated polar surface range of 40.8 Å^2, with a strong contribution from the hydrogen-accepting R-O-R groups of the 1,3-dioxolane and dimethoxyphenyl substructures, except the **2b** ligand, where the R-O$(CH_2)_{11}CH_3$ fragment contributes an additional polar surface of 9.23 Å^2 [32] (Table 1). In the MLP map, it is possible to observe that the Br atom exerts an electron-withdrawing inductive effect that makes the alkyl chain $(CH_2)_3$Br (**1b**) partially hydrophilic, with atomistic lipophilicity indices that vary between −0.08 and 0.06 which, when combined with the hydrophilic effect on the R_3N^+ protic substructure of isoquinoline (green to blue spectra), resulted in a $logD_{pH\ 7.4}$ on the order of −0.3 (Fig. 6a). The same electrophilic region R_3N^+ is responsible for the formation of a hydrophilic surface in the natural product berberine and its alkylated analog **1a**. However, the side chain $(CH_2)_8CH_3$ promotes an extension on the lipophilic surface of compound **1a**, compared to the natural product, resulting in a $logD_{pH\ 7.4}$ on the order of 2.26 (Fig. 6a).

Thus, considering the similar range of polarity between the ligands, the compounds were filtered in a physicochemical space that aligned relative lipophilicity ($logD_{pH\ 7.4}$) and calculated MW (in g/mol) to Pfizer's MPO algorithm to determine the degree of passive permeability of compounds as a function of their structural modifications. On a visual inspection of Fig. 6b, it is possible to observe that the compounds with molecular size lower than 480 g/mol, that is, the lower alkyl chain analogs (berberine, **1a** and **1b**) showed low relative lipophilicity ($logD_{pH\ 7.4} < 3$) and reside in a more favorable physicochemical space with MPO score > 5. It is noteworthy that the berberine compound had the best drug-likeness score (MPO = 6.0), followed by ligands **1b** (MPO = 5.40) and **1a** (MPO = 5.24), as the compounds with the best ADME profile.

3.2. *ADME estimated descriptors*

This systematic decision corroborates the prediction of the ADME descriptors since the compound berberine showed better passive intestinal permeability (P_{app} MDCK = 3.5 × 10^{-5} cm/s), followed by derivative **1b**, with P_{app} MDCK value estimated at 2.5 × 10^{-5} cm/s, and derivative **1a**, with predicted P_{app} MDCK value of 2.0 × 10^{-5} cm/s (Table 2), agreeing with the pharmaceutical classification system of Pfizer's MPO algorithm [33]. In contrast, ligands with $logD_{pH\ 7.4} > 3$ showed the lowest MPO scores and reduction in their passive permeability potential due to the high lipophilicity of their longer alkyl side chains (Fig. 6b). In addition, the high lipophilicity of these compounds makes analogs **1c** ($(CH_2)_{11}CH_3$), **2a** ($(CH_2)_{11}CH_3$) and **2b** (O$(CH_2)_{11}CH_3$) reside outside the spectrum of greater efficiency as ligands, compounds in this range of lipophilicity can reach the CNS [34] (Fig. 7).

The pharmacokinetic spectrum expressed in the heatmap of Fig. 7 is a graphical response of empirical decisions between the predictive tools

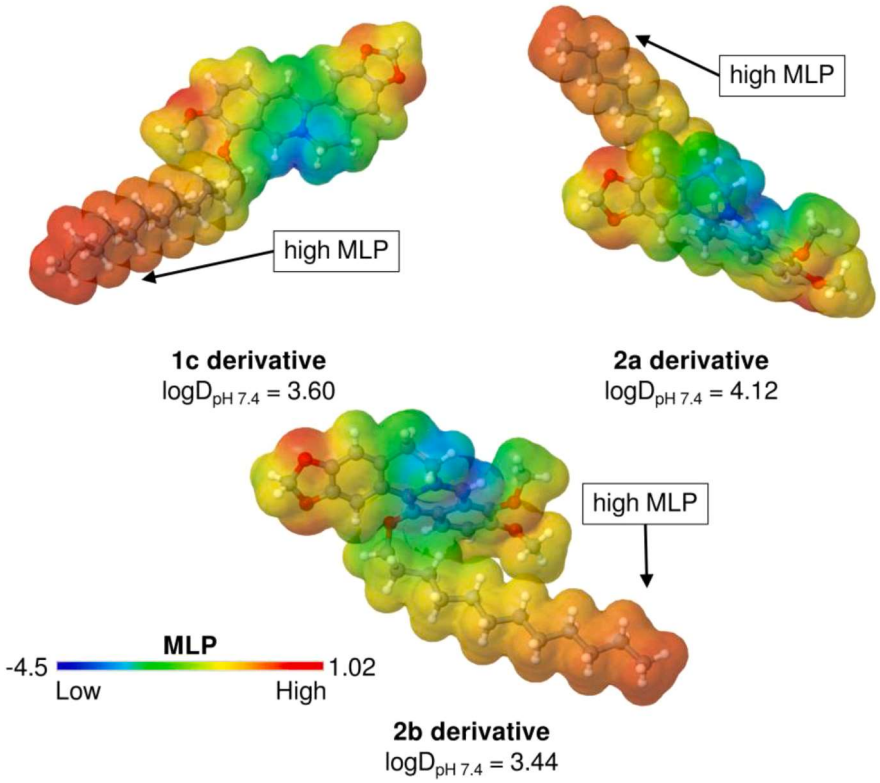

Fig. 5. Molecular lipophilicity potential (MLP) surface map of the most lipophilic ligands (**1c** and **2a-b**).

Table 1
Physicochemical properties of the berberine analogs used in the pharmaceutical classification system from Pfizer's MPO algorithm.

Property	Berberine	Berberine derivatives				
		1a	1b	1c	2a	2b
logP	−1.28	2.26	−0.37	3.60	4.12	3.44
logD	−1.28	2.26	−0.37	3.60	4.12	3.44
MW	336.37 g/mol	448.58 g/mol	443.32 g/mol	490.66 g/mol	504.69 g/mol	520.69 g/mol
TPSA	40.80 Å^2	40.80 Å^2	40.80 Å^2	40.80 Å^2	40.80 Å^2	50.03 Å^2
HBD	0	0	0	0	0	0
pKa	−4.38	−4.39	−4.39	−4.39	−4.38	−4.29
MPO score	6.00	5.24	5.40	3.97	3.44	4.06
Pfizer rule	Accepted	Accepted	Accepted	Rejected	Rejected	Rejected
GT rule	Accepted	Accepted	Accepted	Accepted	Rejected	Rejected

Legend: MW (molecular weight); TPSA (Topological Polar Surface Area); HBD (H-bond donor); MPO (Multiparameter Optimization); GT (Golden Triangle rule).

used. In this, it is possible to observe that compounds **1a-b.** The natural product berberine presents an alignment between high passive permeability ($P_{app} > 10 \times 10^{-6}$ cm/s) and low hepatic clearance ($CL_{int,u} < 50$ mL/$^{min}/_{kg}$), resulting in ranges of GI absorption > 72% and the best estimates of oral bioavailability (F%) around 40% (Table 2). Although the compounds tend to suffer passive efflux by P-gp (+++ token), the low lipophilicity of the compounds with the smallest side chain alkyl (**1a-b**) and berberine has a volume of distribution around 3.8–4.5 L/kg that allows a better uniform distribution of their molecular fractions between blood plasma and biological membranes [35] (Table 2).

3.3. Site of metabolism and toxicity prediction

In the probability map of Fig. 8, it is possible to observe how the metabolism sites are affected by the structural modifications in the generic structure of berberine. In the ADME predictive test, all compounds tended to act as substrates for the CYP2C9 and CYP2D6 isoforms (Fig. 7). With this analysis, it is possible to observe that the alkylbromide substituent linked in the R1 position ($(CH_2)_3Br$), the **1b** analog, performs an electron-withdrawing inductive effect that increases the probability of demethylation of the 1,3-benzodioxole substructure by these CYP450 isoforms. The alkyl group R-$(CH_2)_8CH_3$ reduced the number of O-dealkylation sites in analog **1a**, evidencing the stability of these ligands to pre-systemic metabolism (Fig. 8), constituting one less secondary metabolite in comparison to the class of substituents in the R2 group. On the other hand, alkyl substitutions in the R2 position (**2a-b**) of the isoquinoline substructure return the condition of double O-dealkylation to the generic structure of berberine, resulting in more sites susceptible to pre-systemic metabolism as an indication of low stability metabolic. Corroborating this, it was possible to notice that compounds **1a, 1b** and berberine presented the best clearance spectrum (Fig. 7) predicted by the ADME consensus test.

In this test, it was possible to see that structural modifications based on alkylation decreased the susceptibility of unsaturated centers to undergo epoxidation by aromatic hydroxylation, a hepatotoxic toxicophore, by metabolic activation [36]. This decision corroborates the low risk of hepatotoxicity predicted by the ADME consensus test, as well as the pLC_{50} values ($-\log_{10}LC_{50}$ in mg/L) > 5.0 which infer an indication

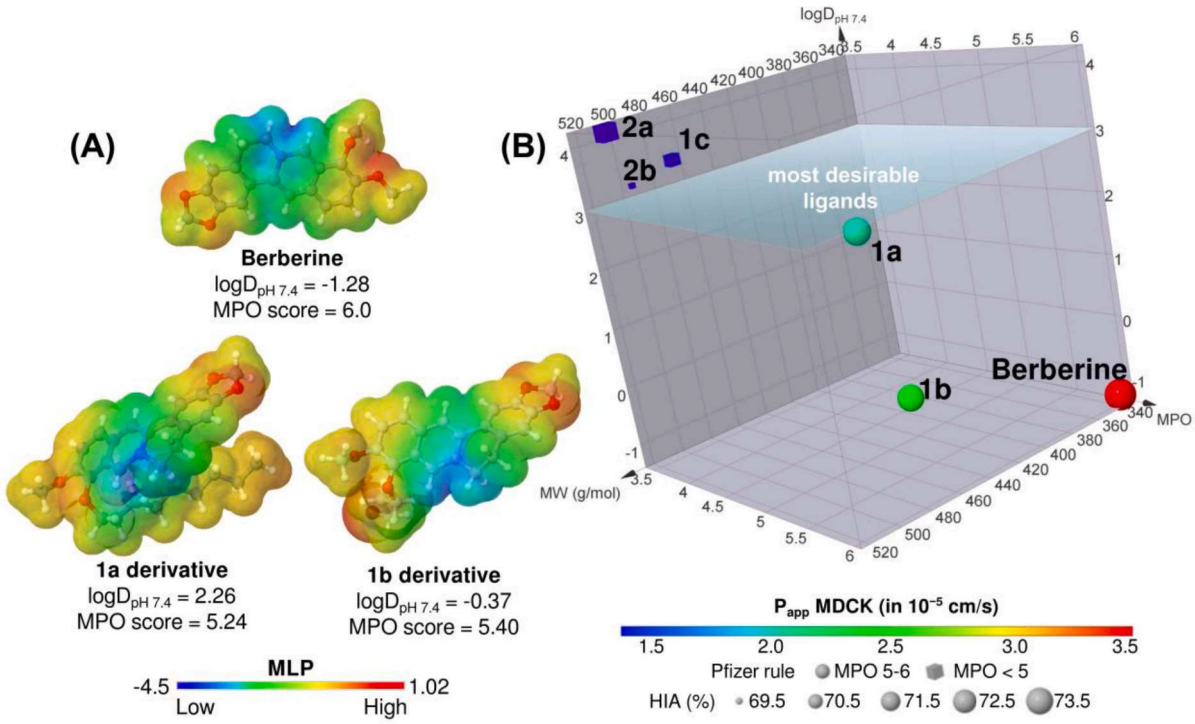

Fig. 6. Molecular lipophilicity potential (MLP) surface map (a) and alignment between physicochemical attributes and pharmacokinetic descriptors of compounds via Pfizer's MPO (b).

Table 2
Pharmacokinetic properties estimated by the ADME consensus test between the ADMETboost – AI Drug Lab – and ADMETlab platforms for berberine derivatives.

Property	Berberine	Berberine derivatives				
		1a	1b	1c	2a	2b
P_{app} rate	3.5×10^{-5} cm/s	2.0×10^{-5} cm/s	2.5×10^{-5} cm/s	1.6×10^{-5} cm/s	1.4×10^{-5} cm/s	1.5×10^{-5} cm/s
P-gp s	+++	+++	+++	+++	+++	+++
GI abs.	73.73%	72.21%	72.23%	70.05%	71.21%	69.31%
F%	44.61%	36.46%	41.75%	32.93%	33.42%	33.33%
VD	3.89 L/kg	4.49 L/kg	4.11 L/kg	4.79 L/kg	4.76 L/kg	4.9 L/kg
CYP2C9	++	++	++	++	+++	+++
CYP2D6	+++	+++	+++	+++	+++	+++
CYP3A4	–	–	–	–	–	–
$CL_{int,u}$	41.09 mL/^{min}/$_{kg}$	49.13 mL/^{min}/$_{kg}$	45.2 mL/^{min}/$_{kg}$	53.59 mL/^{min}/$_{kg}$	52.59 mL/^{min}/$_{kg}$	53.59 mL/^{min}/$_{kg}$
H-HT	—	—	–	—	—	—
pLC_{50}	5.52 mg/L	6.58 mg/L	6.33 mg/L	6.59 mg/L	6.68 mg/L	6.87 mg/L

Legend: P_{app} values were estimated from the *in vitro* test database via MDCK cell line from ADMETlab 2.0. For the classification endpoints, the prediction probability values are transformed into six symbols: 0–0.1(—), 0.1–0.3(–), 0.3–0.5(-), 0.5–0.7(+), 0.7–0.9(++), and 0.9–1.0(+++).

of low acute toxic response (Table 2).

3.4. Evaluation of molecular docking against HIF-1α receptor

After the redocking process with the co-crystallized OGA ligand, the best pose of the ligand fits in an RMSD in the order of 1.176 Å (Table 3), which suggests that the parameterization promotes an excellent binding specificity of the ligand against the HIF-1α receptor [29], in order of free energy (ΔG) = −5.142 kcal/mol which, when compared to the other independent simulations, suggests that the formation of the complex between the ligand and the HIF-1α receptor may require greater energy than system (Fig. 9). Here, it is worth mentioning that ligand **2a** presented the best free energy order at the end of the coupling simulations, with a calculated ΔG value of −8.579 kcal/mol. However, the ADME ligands with the highest viability, i.e., analogs **1a** and **1b** (and the natural product berberine), obtained a final score of −8.04, −7.633 and −7.903 kcal/mol, values that meet the criterion of ideal affinity energy for ligand-receptor complex formation (ΔG < −6.0 kcal/mol) [30].

The calculation of the distances between the ligands and the HIF-1α receptor was associated with the types of interaction with the amino acid residues, which can be seen in Table 3. In a visual inspection of Fig. 10, it is possible to observe that berberine binds from the same catalytic site as the co-crystallized ligand OGA (Fig. 10a), with interactions in common with residues of Gln 147 and Thr 196, with a strong contribution of the isoquinoline substructure (Fig. 10b). The natural product interacts with the Gln 147 residue by H-bond interactions (blue spectrum in the heatmap of Fig. 10c) with a calculated distance of 2.81 Å, characterized as strong ligand-receptor interaction (distance < 3.0 Å) [31], where the ph-OCH_3 group attached to C10 of the protic isoquinoline substructure interacts with the amine group (NH_2) of Gln 147 residue by H-bond interactions (Fig. 10d).

After the cycle of 20 independent simulations for each of the ligands, it was possible to notice that the analogs with better ADME viability, that is, ligands **1a** ($(CH_2)_8CH_3$) and **1b** ($(CH_2)_3Br$), as well as compound **1c** ($(CH_2)_{11}CH_3$), bind to the HIF-1α receptor inhibition site, occupied by the OGA control ligand (Fig. 11a), and showed interactions in

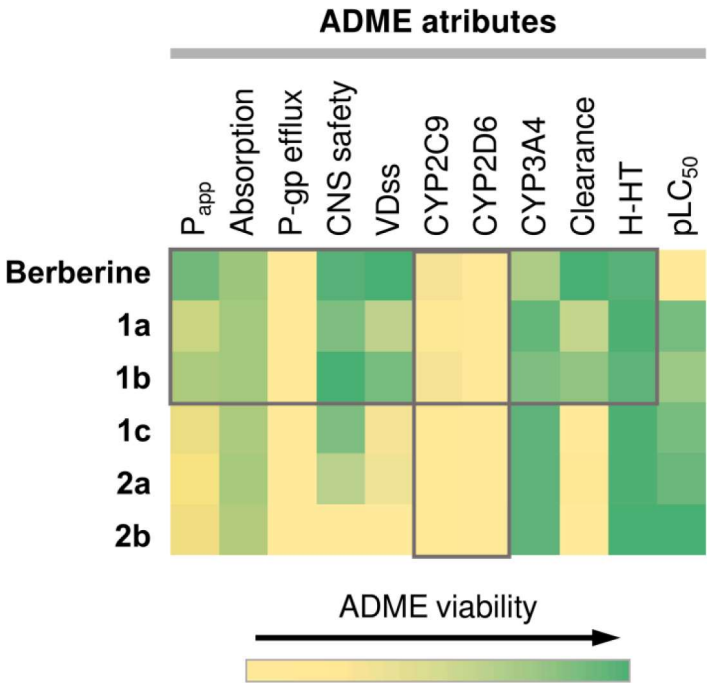

Fig. 7. ADME viability heatmap of berberine derivatives **1a-c** and **2a-b**.

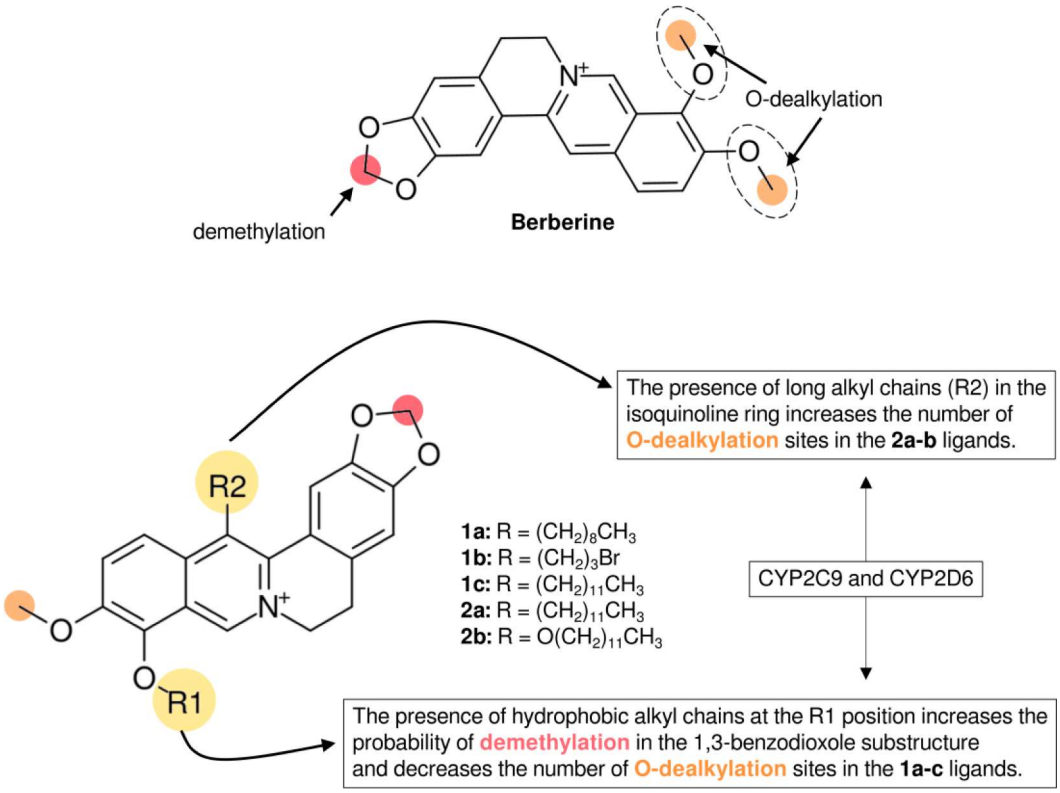

Fig. 8. Metabolism site prediction for the natural product berberine and its synthetic analogs **1a-c** and **2a-b**.

common with Gln 147 and Thr 196 residues (Fig. 11b). The ligands residing in the physicochemical space of greater pharmacokinetic viability showed strong H-bond interactions with the residue of Gln 147 (blue spectrum in the heatmap of Fig. 11c), with distances evaluated at 2.39 Å and 2.49 Å (**1a** and **1b**, respectively), with a contribution from the ph-OCH_3 linked to the protic isoquinoline substructure, similar to the pharmacophore recorded in the previous analysis with the natural product (Fig. 10d). Here, it is important to highlight that, although the alkylbromide side chain positively affects the pharmacokinetics of cellular permeability and metabolic stability of ligand **1b**, it was possible to observe that this side chain resulted in a repulsion effect to the Asn 205 residue (purple colored ligand in Fig. 11b), OGA ligand interaction residue, with calculated distance around 10 Å (Fig. 11c).

Finally, the second class of alkyl compounds substituted at C13 of the

Table 3
Details on interactions between berberine analogs and HIF-1α receptor amino acid residues.

Compound	RMSD	Interactions parameters		
		AA residue	Distance	Type
Berberine*	1.106 Å	Tyr 102	3.86 Å	Hydrophobic
		Trp 296	3.82 Å	Hydrophobic
		Gln 147	2.81 Å	H-bond
		Glu 202	3.18 Å	H-bond
		Gln 203	2.25 Å	H-bond
1a	1.896 Å	Tyr 102	3.42 Å	Hydrophobic
		Tyr 102	3.61 Å	Hydrophobic
		Tyr 102	3.80 Å	Hydrophobic
		Leu 186	3.43 Å	Hydrophobic
		Leu 188	3.73 Å	Hydrophobic
		Phe 207	3.31 Å	Hydrophobic
		Ile 281	3.64 Å	Hydrophobic
		Ile 281	3.42 Å	Hydrophobic
		Trp 296	3.56 Å	Hydrophobic
		Trp 296	3.70 Å	Hydrophobic
		Gln 147	2.39 Å	H-bond
		Glu 202	2.31 Å	H-bond
		Gln 203	2.00 Å	H-bond
1b	1.652 Å	Tyr 102	3.59 Å	Hydrophobic
		Leu 188	3.51 Å	Hydrophobic
		Thr 196	3.76 Å	Hydrophobic
		Trp 296	3.81 Å	Hydrophobic
		Gln 147	2.49 Å	H-bond
		Gln 203	2.86 Å	H-bond
1c	1.102 Å	Tyr 102	3.76 Å	Hydrophobic
		Tyr 102	3.73 Å	Hydrophobic
		Tyr 102	3.75 Å	Hydrophobic
		Leu 186	3.53 Å	Hydrophobic
		Leu 186	3.98 Å	Hydrophobic
		Asp 201	3.93 Å	Hydrophobic
		Glu 202	3.97 Å	Hydrophobic
		Gln 203	3.74 Å	Hydrophobic
		Trp 296	3.75 Å	Hydrophobic
		Trp 296	3.95 Å	Hydrophobic
		Trp 296	3.64 Å	Hydrophobic
		Trp 296	3.75 Å	Hydrophobic
		Gln 147	2.57 Å	H-bond
2a	1.565 Å	Tyr 93	3.62 Å	Hydrophobic
		Tyr 93	3.71 Å	Hydrophobic
		Phe 100	3.61 Å	Hydrophobic
		Tyr 102	3.67 Å	Hydrophobic
		Thr 196	3.51 Å	Hydrophobic
		Trp 296	3.50 Å	Hydrophobic
		Thr 149	2.28 Å	H-bond
		Glu 202	3.08 Å	H-bond
		Glu 202	2.53 Å	H-bond
2b	1.961 Å	Tyr 102	3.47 Å	Hydrophobic
		Leu 186	3.96 Å	Hydrophobic
		Leu 188	3.40 Å	Hydrophobic
		Leu 188	3.95 Å	Hydrophobic
		Thr 196	3.39 Å	Hydrophobic
		Phe 207	3.62 Å	Hydrophobic
		Ile 281	3.76 Å	Hydrophobic
		Trp 296	3.76 Å	Hydrophobic
		Ser 91	2.24 Å	H-bond
		Asp 201	2.81 Å	H-bond
OGA**	1.176 Å	Gln 147	3.51 Å	H-bond
		Gln 147	3.46 Å	H-bond
		Thr 196	2.89 Å	H-bond
		Asn 205	2.92 Å	H-bond
		Asn 294	3.79 Å	H-bond

*natural product;
*co-crystallized inhibitor.

isoquinoline substructure, that is, the berberine analogs **2a** and **2b**, belonging to the class of compounds with lower ADME viability in this study, show weak interactions with the amino acid residues of the site of inhibition in common with OGA, i.e., Gln 147, Thr 196, Asn 205 and Asn 294 (Fig. 12b), where the calculated distances were > 3.0 Å [31] (Fig. 12c). However, they bind at the same site catalytic (Fig. 12a).

4. Discussion

Berberine-derived compounds play a key role in the development of new anticancer drugs. Therefore, studies have been raising efforts to improve the therapeutic effect of berberine from the alkylation of its methoxy centers, as long as this does not cause a decrease in its pharmacokinetic properties, such as passive permeability, efflux and transmembrane transport and metabolic stability [37,38].

A quantitative structure-activity relationship (QSAR) system perfected by Pfizer, Inc., in recent years [39,40] reveals that small and slightly lipophilic compounds (MW < 500 g/mol with logP < 3), provided they are more polar than commercially available CNS-active compounds (TPSA > 40 $Å^2$), show a systematic alignment between three *in vitro* attributes of ADME: high passive permeability (P_{app} MDCK > 10 × 10^{-6} cm/s), low susceptibility to passive efflux by P-gp and low rate of intrinsic clearance of the unbound fraction in the human hepatic system ($CL_{int,u}$ < 100 $mL/^{min}/_{kg}$).

In this study, it was approached that possible alkylations in aromatic centers of the isoquinoline substructure of the generic structure of the natural product berberine could improve its pharmacokinetic effect to enable its anticancer effect. Predictive pharmacokinetic results suggest that compounds with a lower alkyl side chain, that is, the synthetic derivatives **1a-b**, presented a better distribution of their molecular lipophilic surface when compared to analogs with a 12-carbon saturated side chain (**1c, 2a-b**), which infers their occupation in a physicochemical space with better pharmacokinetic alignment. These factors corroborate the estimated ADME descriptors, as they showed excellent passive intestinal permeability and greater metabolic stability. Furthermore, very lipophilic compounds reside outside this physicochemical space and may present risk factors, such as bioaccumulation in biological tissues [41].

Predicting the site of metabolism is a fundamental step in estimating the toxic effects of new prototype substances proposed to be used as an oral drug. This test can relate the degree of specificity of molecular functional groups to phase I metabolism, mediated by CYP450 isoforms, with the sensitivity to being biotransformed by known redox routes of the human liver microsome (HLM) system [42,43]. This prediction allows for establishing relationships between toxic effects and half-life, as these processes mainly infer the clearance route of these drugs [39]. Furthermore, this allows to avoid compounds that form reactive, secondary metabolites, such as compounds based on epoxides, whose hydroxylation in aromatic centers constitute unstable and highly reactive intermediates, whose nucleophilic effect can covalently bind to macromolecules such as proteins and DNA and induce damage to the liver and mutagens [36,44,45].

Demethylation is the metabolic process involving most of the secondary metabolites of berberine, including demethyleneberberine, by demethylation of the benzodioxole substructure, and berberrubine and thalifendine, by O-dealkylation type metabolism of the dimethoxyphenyl substructure [46–48,38,49].

Here, it was possible to observe that substitutions based on alkyl side chains did not even indicate a risk of aromatic hydroxylation, corroborating the indication of low human hepatotoxic response (H—HT) of substances in the ADME predictive test. Furthermore, it was possible to point out that the inductive effect of withdrawing electrons from the alkyl bromide side chain induced the demethylation of the O—CH_2—O fragment of the benzodioxole substructure and reducing the number of O-dealkylation sites, reducing the number of possible metabolites found in the systemic circulation and hepatic clearance.

In a theoretical study of pharmacodynamics recently published by Frota et al., (2022) [26], it was possible to observe that natural polyphenolic biflavonoids showed H-bond interactions, in HIF-1α receptor, in common with the residue of Thr 196, of the catalytic site of the co-crystallized OGA inhibitor, as a strategy for the discovery of new inhibitors of the proliferation of pancreatic cancer cells from natural products. Interestingly, the Thr 196 residue is involved in stabilizing the

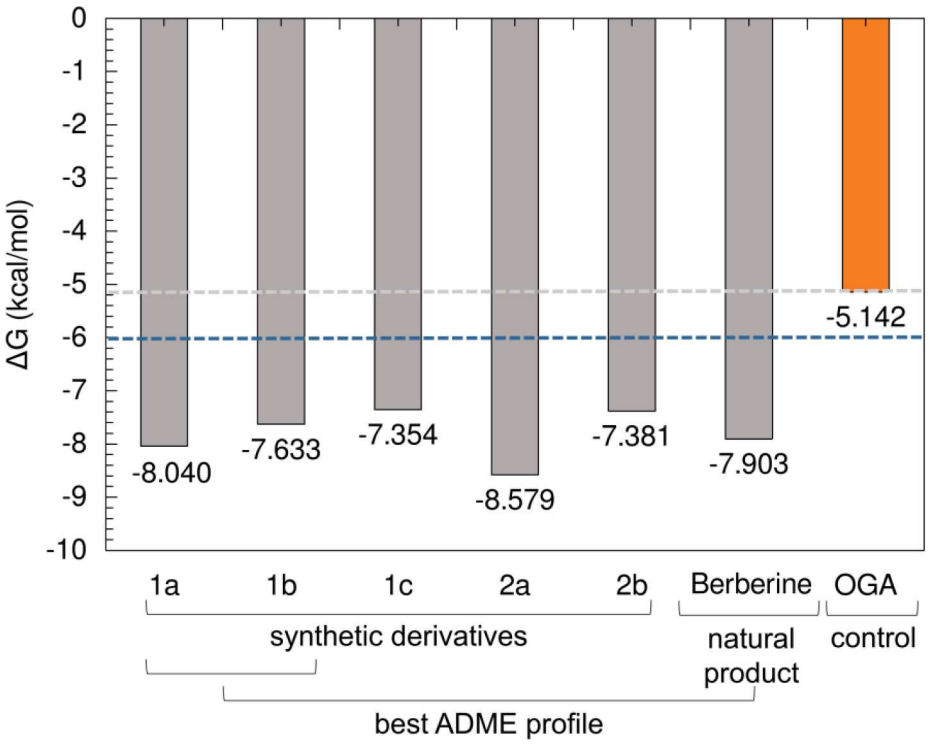

Fig. 9. Calculated values of Gibbs free energy (ΔG) in the formation of ligand-receptor complexes of berberine analogs **1a-c** and **2a-b** against the HIF-1α receptor.

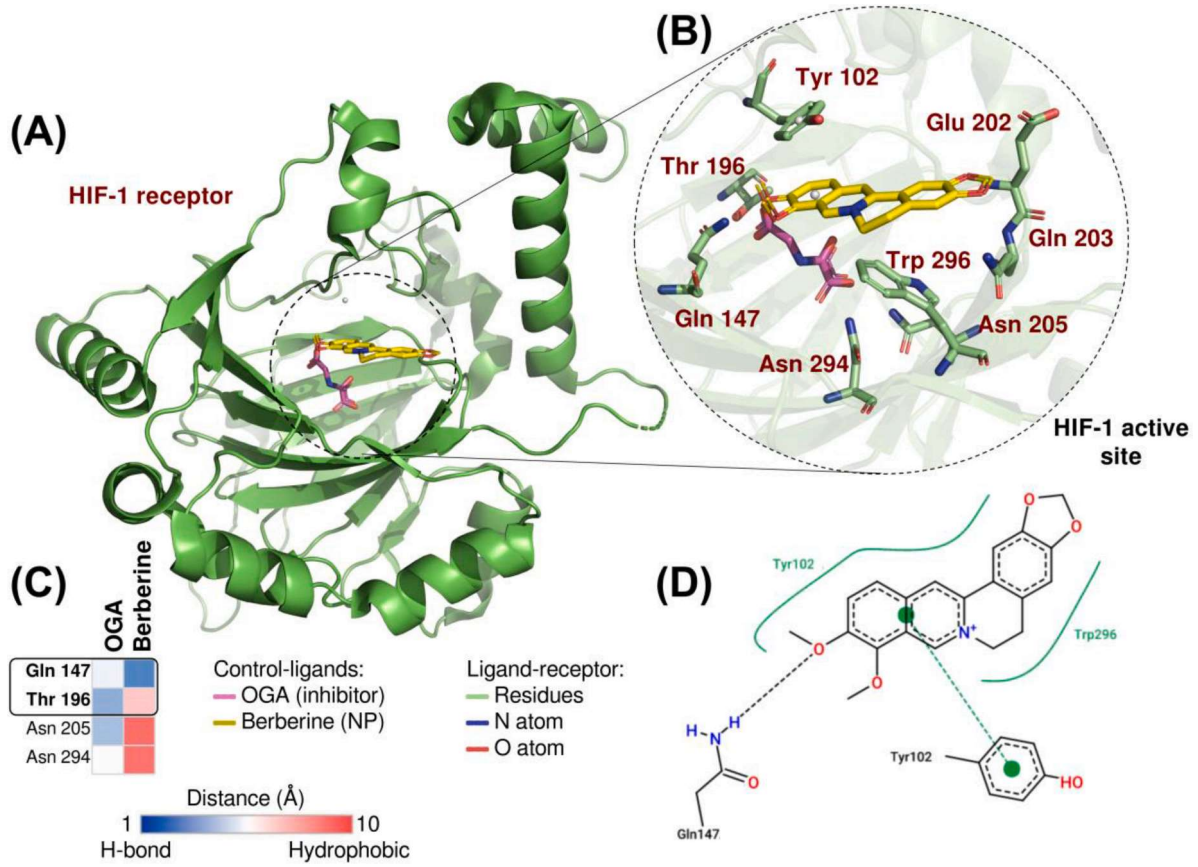

Fig. 10. HIF-1α receptor with highlighted active site (a), co-crystallized inhibitor OGA (magenta) and berberine (yellow) and amino acid residues from the active site (b), heatmap relating distance and type of ligand-receptor interactions (c) and a two-dimensional model showing the H-bond interaction of the ph-OCH_3 group of berberine with the amine group of the Gln 147 residue (d).

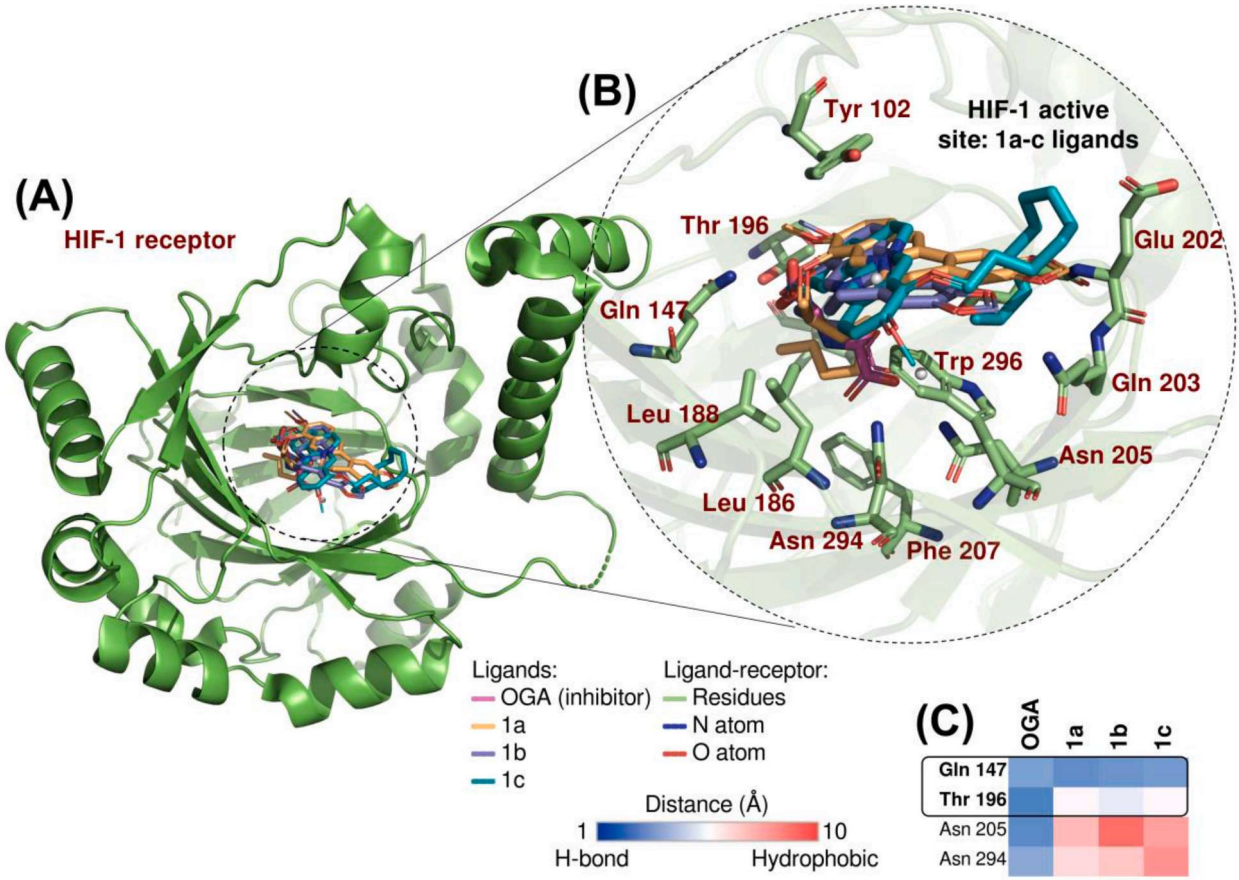

Fig. 11. HIF-1α receptor with highlighted active site (a), co-crystallized OGA inhibitor (magenta) and **1a** (orange), **1b** (purple) and **1c** (cyan) ligands interacting with amino acid residues from the active site (b) and heatmap relating distance and type of ligand-receptor interactions (c).

active site of HIF-1α and constitutes a key point in discovering selective competitive inhibitors in relation to the control ligand OGA [50]. In a study that combines *in vitro* assays and molecular docking, it was possible to notice that structural modifications in coumarin derivatives potentiated the effect of this class of compounds (derived from the natural product coumarin) in the inhibition of the proliferation of HepG2 cells, at the same time that all the synthetic analogs inhibited the HIF-1α target by common interactions with Thr 196 residue [51].

In this study, it was possible to observe that the two classes of substituted derivatives R1 and R2, including the natural product berberine, showed interactions of similar strength with the Thr 196 residue as an indication of competitive inhibition between the ligands. The ligands interact with the residue by H-bond interactions with a strong contribution from their oxygenated groups attached to carbon atoms 9 and 13 in the isoquinoline substructure, showing interactions similar to the carboxyl and carbonyl oxygen groups of the OGA inhibitor ligand [50]. However, the **1a-b** ligands stand out for their pharmacokinetic viability, which, when combined with the optimal affinity energies, estimated at −8.040 kcal/mol and −7.633 kcal/mol (**1a** and **1b**, respectively) [30], constitute candidates for more favorable in the preparation of new prototype HIF-1α inhibitors with low toxic response to the host.

5. Conclusion

In this study, a series of *in silico* pharmacokinetic and pharmacodynamic characterization techniques constitute a multiparametric optimization system to estimate the efficiency of new berberine derivatives against pancreatic cancer via HIF-1α receptor inhibition. From the systematic analysis, it was possible to observe that the less lipophilic ligands, that is, the **1a-b** analogs and the natural product berberine, occupy a physicochemical space with better pharmacokinetic viability, at the same time that the molecular docking simulations demonstrated that they compete for selective and competitive inhibition by the active site of HIF-1α by interactions in common with the residue of Thr 196 and with great affinity energy. However, it is worth noting that future *in vitro* studies with specific cell lines are needed to prove the ligands' effectiveness in treating pancreatic cancer, but this step goes beyond the scope of this study. Thus, this work is an initial study that aims to support future studies of structural modification of berberines in the discovery of new bioactive compounds against pancreatic cancer via modulation of HIF-1α receptors.

Funding

Márcia Machado Marinho acknowledges financial support from the PDCTR (CNPq/Funcap) (Grant#: DCT-0182-00048.02.00/21 e 04879791/2022). Hélcio Silva dos Santos acknowledges financial support from CNPq (Grant#: 306008/2022-0).

Ethical approval

Not applicable.

Consent to participate

Not applicable.

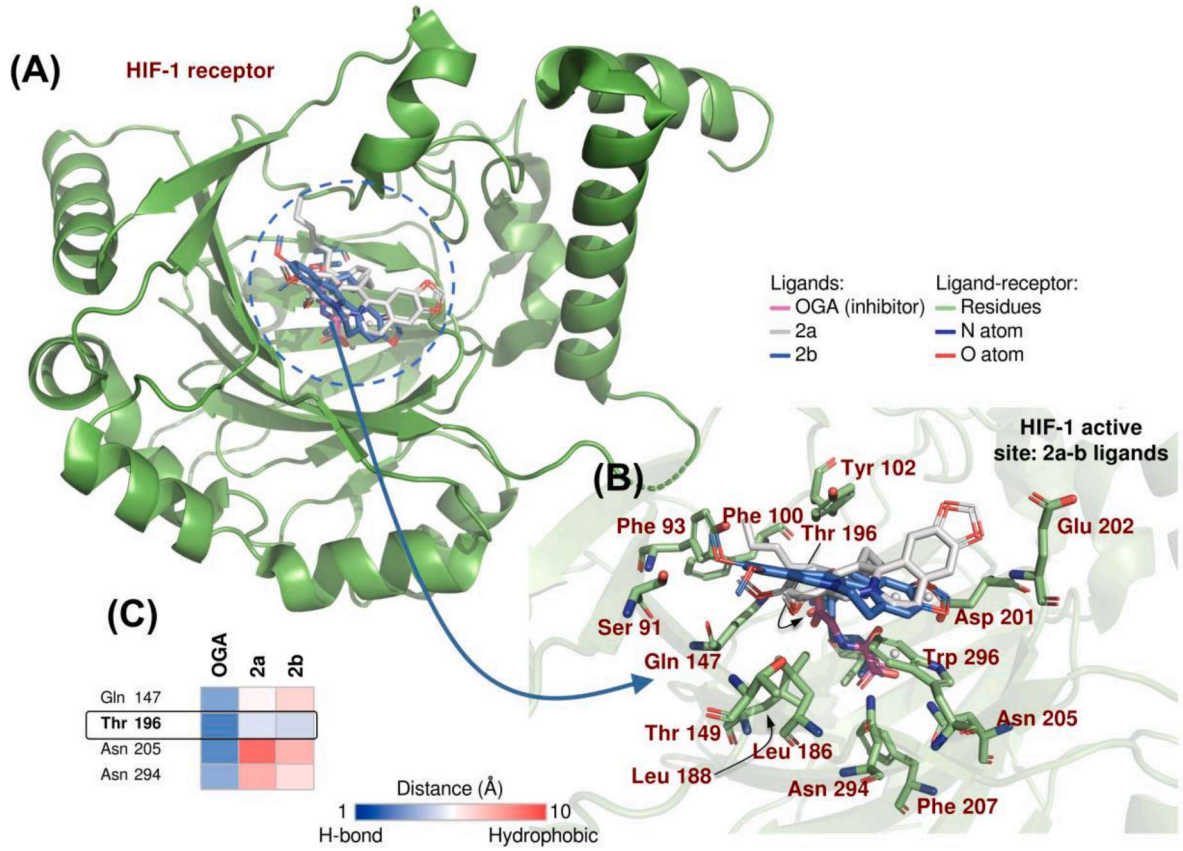

Fig. 12. HIF-1α receptor with highlighted active site (a), co-crystallized OGA inhibitor (magenta) and **2a** (gray) and **2b** (blue) ligands interacting with amino acid residues from the active site (b) and heatmap relating distance and type of ligand-receptor interactions (c).

Consent for publication

Not applicable.

CRediT authorship contribution statement

Matheus Nunes da Rocha: Conceptualization, Data curation, Formal analysis, Funding acquisition, Investigation, Methodology, Visualization, Writing – original draft. **Márcia Machado Marinho:** Conceptualization, Data curation, Formal analysis, Investigation, Methodology, Visualization, Writing – original draft. **Hélcio Silva dos Santos:** Funding acquisition, Project administration, Resources, Supervision, Validation. **Emmanuel Silva Marinho:** Data curation, Project administration, Resources, Supervision, Validation. **Jonas Ildefonso Junior:** Conceptualization, Writing – original draft. **Janini Filgueira Rosas:** Conceptualization, Writing – original draft. **Henrique Douglas Melo Coutinho:** Project administration, Supervision, Validation.

Declaration of Competing Interest

The authors declare that they have no known competing financial interests or personal relationships that could have appeared to influence the work reported in this paper.

Data availability

All data will be available after a reasonable request to the corresponding author.

Acknowledgements

The authors would like to thank to the Brazilian Agencies: Fundação Cearense de Apoio ao Desenvolvimento Científico e Tecnológico (FUNCAP). Conselho Nacional de Desenvolvimento Científico e Tecnológico (CNPq) and Coordenação de Aperfeiçoamento de Ensino Superior (CAPES) for fellowships and financial supports.

References

[1] H. Sung, J. Ferlay, R.L. Siegel, M. Laversanne, I. Soerjomataram, A. Jemal, F. Bray, Global cancer statistics 2020: GLOBOCAN estimates of incidence and mortality worldwide for 36 cancers in 185 countries, CA A Cancer J. Clin. 71 (2021) 209–249, https://doi.org/10.3322/caac.21660.

[2] L.J.H. Brada, M.S. Walma, R.M. van Dam, J. de Vos-Geelen, I.H. de Hingh, G. J. Creemers, M.S. Liem, L.J. Mekenkamp, V.E. de Meijer, D.J.A. de Groot, G. A. Patijn, J.W.B. de Groot, S. Festen, E.D. Kerver, M.W.J. Stommel, M.R. Meijerink, K. Bosscha, J.F. Pruijt, M.B. Polée, J.A. Ropela, G.A. Cirkel, M. Los, J.W. Wilmink, N. Haj Mohammad, H.C. van Santvoort, M.G. Besselink, I.Q. Molenaar, The treatment and survival of elderly patients with locally advanced pancreatic cancer: a post-hoc analysis of a multicenter registry, Pancreatology 21 (2021) 163–169, https://doi.org/10.1016/j.pan.2020.11.012.

[3] T. Kamisawa, L.D. Wood, T. Itoi, K. Takaori, Pancreatic cancer, Lancet 388 (2016) 73–85, https://doi.org/10.1016/S0140-6736(16)00141-0.

[4] V. Goral, Pancreatic cancer: pathogenesis and diagnosis, Asian Pac. J. Cancer Prev. 16 (2015) 5619–5624, https://doi.org/10.7314/APJCP.2015.16.14.5619.

[5] T.J. Grant, K. Hua, A. Singh, Molecular pathogenesis of pancreatic cancer. Progress in Molecular Biology and Translational Science, Elsevier, 2016, pp. 241–275, https://doi.org/10.1016/bs.pmbts.2016.09.008.

[6] P.-C. Hou, Y.-H. Li, S.-C. Lin, S.-C. Lin, J.-C. Lee, B.-W. Lin, J.-P. Liou, J.-Y. Chang, C.-C. Kuo, Y.-M. Liu, H.S. Sun, S.-J. Tsai, Hypoxia-induced downregulation of DUSP-2 phosphatase drives colon cancer stemness, Cancer Res. 77 (2017) 4305–4316, https://doi.org/10.1158/0008-5472.CAN-16-2990.

[7] L. Østergaard, A. Tietze, T. Nielsen, K.R. Drasbek, K. Mouridsen, S.N. Jespersen, M. R. Horsman, The relationship between tumor blood flow, angiogenesis, tumor hypoxia, and aerobic glycolysis, Cancer Res. 73 (2013) 5618–5624, https://doi.org/10.1158/0008-5472.CAN-13-0964.

[8] T. Zhao, H. Ren, J. Li, J. Chen, H. Zhang, W. Xin, Y. Sun, L. Sun, Y. Yang, J. Sun, X. Wang, S. Gao, C. Huang, H. Zhang, S. Yang, J. Hao, LASP1 Is a HIF1α target gene critical for metastasis of pancreatic cancer, Cancer Res. 75 (2015) 111–119, https://doi.org/10.1158/0008-5472.CAN-14-2040.

[9] Y. Wang, Y. Liu, X. Du, H. Ma, J. Yao, The anti-cancer mechanisms of berberine: A review, CMAR 12 (2020) 695–702, https://doi.org/10.2147/CMAR.S242329. Volume.

[10] S. Haider, A.G. Chittiboyina, I.A. Khan, Effective synthetic strategies for the construction of isoquinoline scaffold found in biologically active natural products, COC 22 (2018) 148–164, https://doi.org/10.2174/1385272821666171005150423.

[11] M. Tillhon, L.M. Guamán Ortiz, P. Lombardi, A.I. Scovassi, Berberine: new perspectives for old remedies, Biochem. Pharmacol. 84 (2012) 1260–1267, https://doi.org/10.1016/j.bcp.2012.07.018.

[12] Z. Fang, Y. Tang, J. Ying, C. Tang, Q. Wang, Traditional Chinese medicine for anti-Alzheimer's disease: berberine and evodiamine from evodia rutaecarpa, China Med. 15 (2020) 82, https://doi.org/10.1186/s13020-020-00359-1.

[13] R. Sun, B. Kong, N. Yang, B. Cao, D. Feng, X. Yu, C. Ge, S. Feng, F. Fei, J. Huang, Z. Lu, Y. Xie, C.S. Yang, G.L. Guo, G. Wang, J. Aa, The hypoglycemic effect of berberine and berberrubine involves modulation of intestinal farnesoid X receptor signaling pathway and inhibition of hepatic Gluconeogenesis, Drug Metab. Dispos. 49 (2021) 276–286, https://doi.org/10.1124/dmd.120.000215.

[14] X. Xu, L. Zhang, Y. Zhao, B. Xu, W. Qin, Y. Yan, B. Yin, C. Xi, L. Ma, Antiinflammatory mechanism of berberine on lipopolysaccharideinduced IEC18 models based on comparative transcriptomics, Mol. Med. Rep. 22 (2020) 5163–5180, https://doi.org/10.3892/mmr.2020.11602.

[15] J. Shao, D. Zeng, S. Tian, G. Liu, J. Fu, Identification of the natural product berberine as an antiviral drug, AMB Exp. 10 (2020) 164, https://doi.org/10.1186/s13568-020-01088-2.

[16] S. Kang, Z. Li, Z. Yin, R. Jia, X. Song, L. Li, Z. Chen, L. Peng, J. Qu, Z. Hu, X. Lai, G. Wang, X. Liang, C. He, lizi Yin, The antibacterial mechanism of berberine against *Actinobacillus pleuropneumoniae*, Nat. Prod. Res. 29 (2015) 2203–2206, https://doi.org/10.1080/14786419.2014.1001388.

[17] S. Gaba, A. Saini, G. Singh, V. Monga, An insight into the medicinal attributes of berberine derivatives: a review, Bioorg. Med. Chem. 38 (2021), 116143, https://doi.org/10.1016/j.bmc.2021.116143.

[18] R. Wang, S. Rostyslav, X. Li, H. Lin, X. Zhang, S. Zhang, K. Liu, L. Wang, Synthetic and antitumor comparison of 9-O-alkylated and carbohydrate-modified berberine derivatives, J. Iran Chem. Soc. 17 (2020) 3251–3260, https://doi.org/10.1007/s13738-020-01985-0.

[19] H.-J. Lin, J.-H. Ho, L.-C. Tsai, F.-Y. Yang, L.-L. Yang, C.-D. Kuo, L.-G. Chen, Y.-W. Liu, J.-Y. Wu, Synthesis and In vitro photocytotoxicity of 9-/13-lipophilic substituted berberine derivatives as potential anticancer agents, Molecules 25 (2020) 677, https://doi.org/10.3390/molecules25030677.

[20] N. Oberhauser, A. Nurisso, P.-A. Carrupt, MLP Tools: a PyMOL plugin for using the molecular lipophilicity potential in computer-aided drug design, J. Comput. Aided Mol. Des. 28 (2014) 587–596, https://doi.org/10.1007/s10822-014-9744-0.

[21] T.A. Halgren, Merck molecular force field. I. Basis, form, scope, parameterization, and performance of MMFF94, J. Comput. Chem. 17 (1996) 490–519, https://doi.org/10.1002/(SICI)1096-987X(199604)17:5/6<490::AID-JCC1>3.0.CO;2-P.

[22] Q. Du, G.A. Arteca, Modeling lipophilicity from the distribution of electrostatic potential on a molecular surface, J. Comput.-Aided Mol. Des. 10 (1996) 133–144, https://doi.org/10.1007/BF00402821.

[23] T.T. Wager, X. Hou, P.R. Verhoest, A. Villalobos, Moving beyond Rules: the development of a central nervous system multiparameter optimization (CNS MPO) approach to enable alignment of druglike properties, ACS Chem. Neurosci. 1 (2010) 435–449, https://doi.org/10.1021/cn100008c.

[24] M.N. da Rocha, A.M. da Fonseca, A.N.M. Dantas, H.S. dos Santos, E.S. Marinho, G. S. Marinho, In silico study in mpo and molecular docking of the synthetic drynaran analogues against the chronic tinnitus: modulation of the M1 muscarinic acetylcholine receptor, Mol. Biotechnol. (2023), https://doi.org/10.1007/s12033-023-00748-5.

[25] L. Olsen, M. Montefiori, K.P. Tran, F.S. Jørgensen, SMARTCyp 3.0: enhanced cytochrome P450 site-of-metabolism prediction server, Bioinformatics 35 (2019) 3174–3175, https://doi.org/10.1093/bioinformatics/btz037.

[26] L.S. Frota, M.N. da Rocha, L.L. Bezerra, A.M. da Fonseca, E.S. Marinho, S.M. de Morais, HIF1 inhibition of the biflavonoids against pancreas cancer: drug-likeness, bioavailability, ADMET, PASS, molecular docking, molecular dynamics, and MM/GBSA calculations, J. Biomol. Struct. Dyn. (2022) 1–12, https://doi.org/10.1080/07391102.2022.2112619.

[27] G.M. Morris, R. Huey, W. Lindstrom, M.F. Sanner, R.K. Belew, D.S. Goodsell, A. J. Olson, AutoDock4 and AutoDockTools4: automated docking with selective receptor flexibility, J. Comput. Chem. 30 (2009) 2785–2791, https://doi.org/10.1002/jcc.21256.

[28] O. Trott, A.J. Olson, AutoDock Vina: improving the speed and accuracy of docking with a new scoring function, efficient optimization, and multithreading, J. Comput. Chem. (2009), https://doi.org/10.1002/jcc.21334. NA-NA.

[29] D. Yusuf, A.M. Davis, G.J. Kleywegt, S. Schmitt, An Alternative method for the evaluation of docking performance: RSR vs RMSD, J. Chem. Inf. Model. 48 (2008) 1411–1422, https://doi.org/10.1021/ci800084x.

[30] S. Shityakov, C. Foerster, In Silico Predictive Model to Determine Vector-Mediated Transport Properties For the Blood&Ndash;Brain Barrier Choline Transporter, AABC, 2014, p. 23, https://doi.org/10.2147/AABC.S63749.

[31] A. Imberty, K.D. Hardman, J.P. Carver, S. Perez, Molecular modelling of protein-carbohydrate interactions. Docking of monosaccharides in the binding site of concanavalin A, Glycobiology 1 (1991) 631–642, https://doi.org/10.1093/glycob/1.6.631.

[32] P. Ertl, Polar Surface Area, in: R. Mannhold (Ed.), Methods and Principles in Medicinal Chemistry, 1st ed., Wiley, 2007, pp. 111–126, https://doi.org/10.1002/9783527621286.ch5.

[33] T.T. Wager, R.Y. Chandrasekaran, X. Hou, M.D. Troutman, P.R. Verhoest, A. Villalobos, Y. Will, Defining desirable central nervous system drug space through the alignment of molecular properties, in Vitro ADME, and safety attributes, ACS Chem. Neurosci. 1 (2010) 420–434, https://doi.org/10.1021/cn100007x.

[34] J.D. Hughes, J. Blagg, D.A. Price, S. Bailey, G.A. DeCrescenzo, R.V. Devraj, E. Ellsworth, Y.M. Fobian, M.E. Gibbs, R.W. Gilles, N. Greene, E. Huang, T. Krieger-Burke, J. Loesel, T. Wager, L. Whiteley, Y. Zhang, Physiochemical drug properties associated with in vivo toxicological outcomes, Bioorg. Med. Chem. Lett. 18 (2008) 4872–4875, https://doi.org/10.1016/j.bmcl.2008.07.071.

[35] D.E.V. Pires, L.M. Kaminskas, D.B. Ascher, Prediction and optimization of pharmacokinetic and toxicity properties of the ligand, in: M. Gore, U.B. Jagtap (Eds.), Computational Drug Discovery and Design, Springer New York, New York, NY, 2018, pp. 271–284, https://doi.org/10.1007/978-1-4939-7756-7_14.

[36] T.B. Hughes, G.P. Miller, S.J. Swamidass, Modeling epoxidation of drug-like molecules with a deep machine learning network, ACS Cent. Sci. 1 (2015) 168–180, https://doi.org/10.1021/acscentsci.5b00131.

[37] C.-S. Liu, Y.-R. Zheng, Y.-F. Zhang, X.-Y. Long, Research progress on berberine with a special focus on its oral bioavailability, Fitoterapia 109 (2016) 274–282, https://doi.org/10.1016/j.fitote.2016.02.001.

[38] X.-S. Tan, J.-Y. Ma, R. Feng, C. Ma, W.-J. Chen, Y.-P. Sun, J. Fu, M. Huang, C.-Y. He, J.-W. Shou, W.-Y. He, Y. Wang, J.-D. Jiang, Tissue distribution of berberine and its metabolites after oral administration in rats, PLoS ONE 8 (2013) e77969, https://doi.org/10.1371/journal.pone.0077969.

[39] T.W. Johnson, K.R. Dress, M. Edwards, Using the Golden Triangle to optimize clearance and oral absorption, Bioorg. Med. Chem. Lett. 19 (2009) 5560–5564, https://doi.org/10.1016/j.bmcl.2009.08.045.

[40] T.T. Wager, X. Hou, P.R. Verhoest, A. Villalobos, Central nervous system multiparameter optimization desirability: application in drug discovery, ACS Chem. Neurosci. 7 (2016) 767–775, https://doi.org/10.1021/acschemneuro.6b00029.

[41] S.K. Bhal, K. Kassam, I.G. Peirson, G.M. Pearl, The rule of five revisited: applying log *D* in place of Log *P* in drug-likeness filters, Mol. Pharm. 4 (2007) 556–560, https://doi.org/10.1021/mp0700209.

[42] P. Rydberg, U. Ryde, L. Olsen, Sulfoxide, sulfur, and nitrogen oxidation and dealkylation by cytochrome P450, J. Chem. Theory Comput. 4 (2008) 1369–1377, https://doi.org/10.1021/ct800101v.

[43] M. Zheng, X. Luo, Q. Shen, Y. Wang, Y. Du, W. Zhu, H. Jiang, Site of metabolism prediction for six biotransformations mediated by cytochromes P450, Bioinformatics 25 (2009) 1251–1258, https://doi.org/10.1093/bioinformatics/btp140.

[44] A.K. Basu, J.M. Essigmann, Establishing linkages among DNA damage, mutagenesis, and genetic diseases, Chem. Res. Toxicol. 35 (2022) 1655–1675, https://doi.org/10.1021/acs.chemrestox.2c00155.

[45] K. Yu, X. Geng, M. Chen, J. Zhang, B. Wang, K. Ilic, W. Tong, High daily dose and being a substrate of cytochrome P450 enzymes are two important predictors of drug-induced liver injury, Drug Metab. Dispos. 42 (2014) 744–750, https://doi.org/10.1124/dmd.113.056267.

[46] Y. Guo, F. Li, X. Ma, X. Cheng, H. Zhou, C.D. Klaassen, CYP2D plays a major role in berberine metabolism in liver of mice and humans, Xenobiotica 41 (2011) 996–1005, https://doi.org/10.3109/00498254.2011.597456.

[47] Y. Li, G. Ren, Y.-X. Wang, W.-J. Kong, P. Yang, Y.-M. Wang, Y.-H. Li, H. Yi, Z.-R. Li, D.-Q. Song, J.-D. Jiang, Bioactivities of berberine metabolites after transformation through CYP450 isoenzymes, J. Transl. Med. 9 (2011) 62, https://doi.org/10.1186/1479-5876-9-62.

[48] Y. Liu, H. Hao, H. Xie, H. Lv, C. Liu, G. Wang, Oxidative demethylenation and subsequent glucuronidation are the major metabolic pathways of berberine in rats, J. Pharm. Sci. 98 (2009) 4391–4401, https://doi.org/10.1002/jps.21721.

[49] P.-L. Tsai, T.-H. Tsai, Hepatobiliary excretion of berberine, Drug Metab. Dispos. 32 (2004) 405–412, https://doi.org/10.1124/dmd.32.4.405.

[50] C.E. Dann, R.K. Bruick, Dioxygenases as O2-dependent regulators of the hypoxic response pathway, Biochem. Biophys. Res. Commun. 338 (2005) 639–647, https://doi.org/10.1016/j.bbrc.2005.08.140.

[51] B. Manjunatha, Y.D. Bodke, H.M. Kumaraswamy, P. Meghana, O. Nagaraja, G. C. Anjan kumar, Novel thioether linked 4-hydroxycoumarin derivatives: synthesis, characterization, in vitro pharmacological investigation and molecular docking studies, J. Mol. Struct. 1249 (2022), 131642, https://doi.org/10.1016/j.molstruc.2021.131642.